NMR Structure of a Gemcitabine-Substituted Model Okazaki Fragment†

David Konerding,‡ Thomas L. James,§ Eric Trump,|| Ana Maria Soto,⊥ Luis A. Marky,⊥ and William H. Gmeiner*,#

Graduate Group in Biophysics and Department of Pharmaceutical Chemistry, University of California at San Francisco, San Francisco, California 94143, Department of Chemistry, Emporia State University, Emporia, Kansas 66801, Department of Pharmaceutical Sciences, University of Nebraska, Omaha, Nebraska 68198, and Department of Biochemistry, Wake Forest University School of Medicine, Winston-Salem, North Carolina 27157

Received August 13, 2001; Revised Manuscript Received October 12, 2001

ABSTRACT: Gemcitabine (2′-deoxy-2′,2′-difluorodeoxycytidine; dFdC) is a potent anticancer drug that exerts cytotoxic activity, in part, through incorporation of the nucleoside triphosphate dFdCTP into DNA and perturbations to DNA-mediated processes. The structure of a model Okazaki fragment containing a single dFdC substitution, [GEM], was determined using NMR spectroscopy and restrained molecular dynamics to understand structural distortions that may be induced in replicating DNA resulting from dFdC substitution. The electrostatic surface of [GEM] was also computed to determine how the geminal difluoro group of dFdC perturbs DNA electrostatics. The stability of [GEM] was investigated using temperature-dependent UV spectroscopy. dFdC adopted a C3′-endo conformation in [GEM] and decreased the melting temperature of the duplex by 4.3 °C. dFdC substitution did not decrease helical stacking among adjacent purines in the DNA duplex region. dFdC substitution substantially altered the electrostatic properties of the model Okazaki fragment, with increased electron density in the vicinity of the geminal difluoro group. The results are consistent with dFdC substitution altering the structural, electrostatic, and thermodynamic properties of DNA and interfering in DNA-mediated processes. Interference in DNA-mediated processes due to dFdC substitution likely contributes to the anticancer activity of dFdC.

Gemcitabine [2′-deoxy-2′,2′-difluorodeoxycytidine (dFdC); Figure 1] is one of the most widely used and efficacious anticancer drugs in current use. dFdC, either as a single agent or in combination chemotherapy, has demonstrated efficacy toward several of the most prevalent human cancers, including breast (*1*), ovarian (*2*), and lung cancers (*3*). dFdC is also one of the most widely used anticancer drugs for treatment of the most devastating human cancers for which no adequate treatment options are available. For example, dFdC is used in the treatment of pancreatic cancer (*4*) and in the treatment of mesothelioma (*5*). dFdC is active as a single agent (*6*) and also has been shown to possess palliative effects in cancer patients (*7*). dFdC is most frequently used, however, in combination chemotherapy regimens (*8*). dFdC is frequently combined effectively with cisplatin (*9*, *10*), and the extent of platinum−DNA adduct formation positively correlates with the level of incorporation of dFdC into DNA (*11*). dFdC is also used effectively in combination with topotecan (*2*), a potent inhibitor of DNA topoisomerase I (top1). The effectiveness of chemotherapeutic combinations

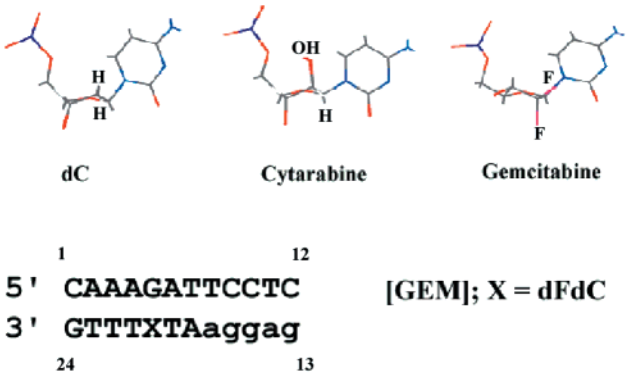

FIGURE 1: Structure of 2′-deoxycytidine (dC), cytarabine, and gemcitabine (dFdC). The nucleotides are shown in the same conformation each adopted in the final, refined NMR structures of [OKA] (*24*), [ARAC] (*24*), and [GEM]. The sequence of the model Okazaki fragment investigated in these studies is shown at the bottom of the figure. Deoxyribonucleotides are indicated in upper case letters and ribonucleotides in lower case letters. The position of dFdC substitution in [GEM] is indicated by an X.

combining dFdC with a drug that damages DNA, or interferes with DNA-mediated processes, suggests that the anticancer activity of dFdC is substantially due to the misincorporation of dFdCTP into DNA. In this paper, the effects of dFdC substitution on the structure, stability, and electrostatics of a model Okazaki fragment are described (Figure 1).

dFdC is a deoxycytidine (dC) analogue that is a member of the antimetabolite class of anticancer drugs (*8*). dFdC requires metabolic activation to the nucleoside diphosphate (dFdCDP) and triphosphate (dFdCTP) forms to exert its

† Supported by NIH NCI CA60612 and P30 CA12197 (W.H.G.), NIH RR01081 and NIH GM39247 (D.K. and T.L.J.), and NIH GM42223 (L.A.M.).

* To whom correspondence should be addressed. Phone: (336) 716-6216. Fax: (336) 716-7671. E-mail: bgmeiner@wfubmc.edu.

‡ Graduate Group in Biophysics, University of California at San Francisco.

§ Department of Pharmaceutical Chemistry, University of California at San Francisco.

|| Emporia State University.

⊥ University of Nebraska.

Wake Forest University School of Medicine.

10.1021/bi015678l CCC: $22.00
Published on Web 12/20/2001

cytotoxic effects (*12*, *13*). The cellular targets of dFdCDP and dFdCTP include DNA polymerases, ribonucleotide reductase, and CTP synthase. Biochemical studies demonstrate that dFdCTP is incorporated predominantly into DNA, with little incorporation into RNA (*14*). dFdCTP is a poor substrate for human DNA polymerases, however, with an efficiency of incorporation only ~5% that of dCTP (*15*). A strong correlation has been shown between incorporation of dFdCTP into DNA and the loss of viability of cells, as determined using a clonogenic assay (*14*). Once dFdCTP is incorporated into DNA, the polymerase adds one additional nucleotide after which the polymerase pauses (*15*). The effects of dFdCTP incorporation into DNA on further chain elongation are complex and are not currently understood in physicochemical detail. dFdC is found predominantly in internucleotide linkages in DNA (*15*). dFdC is also a potent sensitizer to radiation, an activity that requires metabolism to dFdCTP and incorporation into DNA (*16*).

In addition to the DNA-directed effects of dFdC, dFdC also extensively modulates CTP and dCTP metabolism (*17*). dFdC reduces cellular concentrations of CTP and dCTP 5% and 50%, respectively, apparently by blocking the activity of CTP synthase. Cellular depletion of CTP and dCTP inhibits DNA replication and RNA synthesis, respectively, in cells exposed to dFdC. Reduction in dCTP pools also enhances the misincorporation of dFdCTP into DNA by increasing the dFdCTP:dCTP ratio. In this respect, the activity of the drug is self-potentiating with the non-DNA-directed effects serving to enhance misincorporation of dFdCTP into DNA, thus enhancing the DNA-mediated effects of the drug (*8*). dFdCTP also inhibits dCMP deaminase, leading to decreased catabolism of dFdC (*12*). This unique, self-potentiating activity of dFdC is thought to be responsible, in part, for the superior antitumor activity of dFdC relative to other nucleoside analogues used for the treatment of cancer.

Perturbations to DNA structure appear to play a significant role in the anticancer activity of nucleoside analogues such as arabinofuranosylcytosine (cytarabine) and 5-fluorouracil (5-FU). For example, cytarabine, a dC analogue that has potent antileukemic activity, has been shown to interfere with top1-mediated cleavage of duplex DNA (*18*). Cytarabine misincorporation has also been shown to inhibit lagging strand DNA replication and to cause DNA strand breaks to occur at sites distal relative to the site of misincorporation (*19*, *20*). The thymidine triphosphate (dTTP) analogue FdUTP, a metabolite of the widely used anticancer drug 5-FU, may be misincorporated into DNA, and the substituted DNA is a substrate for the DNA mismatch repair machinery, suggesting fluoropyrimidine substitution perturbs DNA structure (*21*). Our laboratory has investigated the structural consequences of nucleotide analogue substitution in DNA using NMR spectroscopy (*22*). We recently investigated the structural basis for alterations in lagging strand replication due to cytarabine misincorporation by determining the NMR structure of a cytarabine-substituted model Okazaki fragment (*23*, *24*). These studies revealed that cytarabine substitution into the DNA duplex region of the model Okazaki fragment resulted in local distortion of the DNA duplex and increased global curvature of the model Okazaki fragment. We have also shown that FdU substitution perturbs the structure and stability of duplex DNA (*25*, *26*). These results are consistent with direct structural perturbations to DNA duplex structure arising from nucleotide analogue misincorporation as being responsible for the DNA-mediated effects of the anticancer drugs cytarabine and 5-FU.

The anticancer activity of dFdC, like cytarabine and 5-FU, may result, in part, from perturbation of DNA-mediated processes that occur due to changes in the structure of the DNA as a consequence of dFdCTP misincorporation. The effects of dFdCTP misincorporation to the structure of duplex DNA have not been as extensively studied as for cytarbine and 5-FU, anticancer drugs that have been in clinical use for considerably longer. The geminal difluoro group of dFdC likely perturbs the electrostatic surface of duplex DNA into which dFdCTP has been misincorporated in a nonsequence selective manner. These electrostatic effects might alter cognate protein binding and may be a significant factor in the altered kinetics of dFdCTP misincorporation (relative to dCTP) and for the pause in polymerase activity following dFdCTP misincorporation (*15*). Alterations to the structure of duplex DNA due to dFdCTP misincorporation likely also contribute to perturbations in DNA processing. At present, few structural data are available concerning the effects of dFdC substitution on DNA structure. We have determined the NMR structure of a dFdC-substituted model Okazaki fragment ([GEM]; Figure 1) in order to evaluate the perturbation to duplex DNA structure resulting from dFdC substitution. The model Okazaki fragment studied had the same sequence as that previously used to investigate the effects of cytarbine misincorporation to DNA structure (*23*, *24*). Use of the same sequence facilitates direct comparison between the structural perturbations caused by the two dC analogues. The conformation of dFdC in [GEM] is markedly different from either cytarabine or dC in the same model Okazaki fragment sequence. Unlike cytarabine, however, the distorted nucleoside structure of dFdC is accommodated well into the same global solution structure as the native model Okazaki fragment. The results are consistent with perturbations to DNA-mediating processes due to dFdCTP misincorporation resulting from both altered local structure to the DNA duplex and changes in the electronic configuration of the nucleotide.

MATERIALS AND METHODS

Preparation of Gemcitabine Phosphoramidite. The phosphoramidite of dFdC [5′-*O*-(4,4′-dimethoxytrityl)-3′-*O*-(2-cyanoethyl)-*N*,*N*-diisopropylphosphoramidite−N_4-benzoyl-2′-deoxy-2,2′-difluorocytidine] was synthesized in a manner similar to that previously described (*27*). All reactions were carried out under argon in flame-dried glassware. Pyridine was distilled over calcium hydride and under argon prior to use. Gemcitabine was a gift (to W. H. Gmeiner) from Eli Lilly. All other reagents were obtained from Aldrich. The intermediate amino-protected compound N_4-benzoyl-2′-deoxy-2′,2′-difluorocytidine was prepared from the hydrochloride salt of gemcitabine by reaction with benzoyl chloride in pyridine with transient protection of the deoxyribose hydroxyls with trimethylsilyl chloride. The tritylated intermediate [5′-*O*-(4,4′-dimethoxytrityl)-N_4-benzoyl-2′-deoxy-2′,2′-difluorocytidine] was prepared by subsequent reaction with 4,4′-dimethoxytrityl chloride using standard methods. Gemcitabine phosphoramidite was then prepared by reaction with 2-cyanoethyl-*N*,*N*′-diisopropylchlorophosphoramidite in

anhydrous tetrahyrofuran with diisopropylethylamine as base. The resulting 5′-*O*-dimethoxytrityl-3′-*O*-phosphoramidite was purified by column chromatography and incorporated in place of one deoxycytidine (dFdC20; see Figure 1) during the chemical synthesis of the RNA/DNA hybrid strand of [GEM].

The oligonucleotides for the model Okazaki fragment containing dFdC were synthesized using an ABI 394 synthesizer in the Molecular Biology Core Laboratory at the Eppley/UNMC Cancer Center. The sequences for the DNA strand and the hybrid DNA/RNA strand, which included the site of dFdC substitution, are shown in Figure 1. The sequences selected were identical, other than the site of dFdC substitution, to the model Okazaki sequences previously investigated by our laboratory (*23*, *24*). Oligonucleotide synthesis was similar to that previously described for the cytarbine-substituted model Okazaki fragment except 4,5-dicyanoimidazole was used as activator and TOM-protected RNA amidites were used with a 6 min coupling time. Deprotection of RNA and DNA was accomplished using 2 mL of 40% aqueous methylamine and 2 mL of 33% ethanolic methylamine for each 10 μmol scale synthesis, followed by incubation at room temperature for 6−8 h. The solution was evaporated to dryness, 4 mL of tetrabutylammonium fluoride was added, and the mixture was heated to 50 °C until the oligonucleotide dissolved followed by slow cooling. The oligonucleotides were HPLC purified using a Waters Delta-Prep 4000 with a Hamilton PRP-1 polystyrene semipreparative column. A 30 min linear gradient with initial conditions of 96% buffer A (0.1 M TEAA) and 4% buffer B (80% aqueous acetonitrile) and final conditions of 80% buffer A and 20% buffer B was used for oligonucleotide purification.

Temperature-Dependent UV Spectroscopy. Absorbance versus temperature profiles (melting curves) were measured with a thermoelectrically controlled Aviv 14-DS spectrophotometer. The absorbance was monitored at 260 nm, and the temperature was scanned at a heating rate of 0.5 °C/min. Analysis of the resulting melting curves, using an all or none approximation, allowed measurement of transition temperatures, T_M, which are the midpoint temperatures of the helix−coil transition of the duplex and van't Hoff enthalpies, ΔH_{vH}. The ΔH_{vH}'s were obtained in two different ways, from shape analysis of the melting curves and from the T_M dependence on strand concentration, using the equation:

$$1/T_M = R/\Delta H_{vH} \ln(C_T/4) + \Delta S/\Delta H_{vH}$$

where C_T is the total concentration of strands and R is the gas constant (*28*). The concentration of each oligomer was determined at 260 nm and 80 °C, using extinction coefficients of 120.6 and 119.3 mM^{-1} cm^{-1} for [OKA] and [GEM], respectively. These values were calculated by extrapolating the tabulated values of dimer and monomer bases at 25 °C (*29*) to high temperatures, using procedures reported earlier (*30*). ΔS and ΔH were calculated from the latter equation while ΔG was calculated from the Gibbs equation: $\Delta G = \Delta H - T\Delta S$. All experiments were conducted in buffers containing 10 mM sodium cacodylate and 100 mM sodium chloride, adjusted to pH 7.

NMR Spectroscopy. NMR experiments were performed using a Varian UNITY 500 NMR spectrometer at the Eppley/UNMC Cancer Center. Samples for NMR analysis were prepared by mixing equimolar amounts of the DNA strand and the hybrid DNA/RNA strand. Sample concentration was approximately 1 mM duplex in 600 μL of 2 mM sodium cacodylate (pH 7.3), 100 mM NaCl, and 0.2 mM Na_2EDTA. ^1H spectra were acquired using a $^1H\{^{13}C,^{15}N\}$ 5 mm PFG probe (Varian, Inc.) and were referenced to HDO at 4.76 ppm at 26 °C. 1D ^1H NMR spectra in 95% H_2O (5% D_2O) at 26, 29, 32, 35, and 38 °C were obtained using a 1-3-3-1 binomial pulse for water suppression (*31*). 2D NOESY spectra in 95% H_2O solution were acquired using a 1-1 echo pulse sequence for water suppression. All spectra in H_2O were acquired with an 11 kHz spectral window centered about the ^1HDO resonance. NOESY spectra in D_2O were acquired for mixing times of 100, 150, and 200 ms using the standard three-pulse sequence using States' method of phase cycling for pure absorption spectra (*32*). Four hundred free induction decays, 16 scans each, with alternating block acquisition, were collected in the t_1 dimension. A total of 2048 data points over a 5000 Hz spectral window were collected in the t_2 dimension with the carrier frequency set at the ^1HDO resonance. A relaxation delay of 8 s was included between scans to allow sufficient relaxation for cross-peak quantitation. TOCSY spectra were acquired with 60 and 100 ms mix times using parameters similar to those used for NOESY spectra, except the relaxation delay was shortened to 3 s. ECOSY spectra were collected using 32 scans per increment with a 3 s relaxation delay and 4096 points in t_2 (*33*). All data were initially processed with VNMR version 5.3B from Varian and then imported into SPARKY (UCSF) for analysis. The spectra were apodized using shifted Gaussian filter functions. After zero-filling in the t_1 dimension, the final matrices were 2048 × 2048 points, except for ECOSY spectra which were 4096 × 2048 points. T_1 and T_2 data were obtained from inversion/recovery and CPMG experiments, respectively, and were fit to single-exponential functions using VNMR 5.3B. 1D ^{19}F and 2D $^1H-^{19}F$ HOESY spectra were acquired using a Nalorac 5 mm $^1H/^{19}F$ probe. $^1H-^{19}F$ HOESY spectra were acquired using 5000 Hz spectral windows for both ^1H and ^{19}F with 1024 points in t_2 and 256 points in t_1 (*34*).

Experimental Constraints. Constraints on interproton distances were determined from NOESY data sets in D_2O solution. Interproton distances were calculated from NOESY cross-peak intensities using MARDIGRAS (*35*). Volume integrals were evaluated from NOESY experiments acquired with 100, 150, and 200 ms mix times, respectively. NOESY intensities evaluated for cross-peaks on both sides of the diagonal were averaged. A complete relaxation matrix was created for [GEM] using intensities evaluated experimentally for 364 interproton interactions and estimated intensities from the geometry of the starting structure for those interproton interactions that could not be evaluated from the experimental data. The diagonal and off-diagonal terms were compared iteratively until the sum of the residual errors was minimized. MARDIGRAS calculations for [GEM] were carried out with three experimental data sets (100, 150, 200 ms), two geometries for the initial structure (A- and B-form double helices), and three values for the isotropic correlation time (τ_c = 1.1, 1.4, and 1.7 ns). Estimates of interproton distances associated with NOE cross-peak intensities resulting from each of the 18 MARDIGRAS calculations for each duplex

were averaged. The average distance and standard deviation were then used to set the flat portion of the potential well for each distance constraint. Estimates of $^3J_{HH}$ from ECOSY spectra for the deoxyribonucleotides in [GEM] were the same, within experimental uncertainty, as those measured previously for [OKA]. Thus the torsion angle restraints used previously in the refinement of [OKA] were used in the refinement of [GEM]. The restraint file used in refinement of [GEM] is included in Supporting Information.

Molecular Refinement. Molecular graphics images were produced using the Chimera package from the Computer Graphics Laboratory, University of California, San Francisco (*36*). The electrostatic charge parameters for the GEM residue were determined as follows. The GEM residue was built as a model starting from dC with the LEaP module of AMBER (*37*). The H2′1 and H2′2 atoms were replaced with F2′1 and F2′2 atoms, and the resulting model was input into Gaussian98 for optimization and electrostatic potential calculation. The esp data from Gaussian were used to generate point charges for the entire residue using the program ANTECHAMBER (*38*). The point charges were very similar to those of the dC residue. Fluorine charges were treated as equivalent during the RESP fit and were calculated to be −0.2403 (H2′1 and H2′2 are 0.0718). The GEM residue was built with LEaP and then minimized using the fluorine charges and the fluorine bond parameters (F−CT−CT, 50.0 kcal/mol bond constant, optimal angle 109°).

The structure refinement of [GEM] (Figure 1) was performed as follows. Two initial models of [GEM] were created: one in canonical A-form and the other in canonical B-form. The initial models were charge-neutralized with hydrated sodium ions (*39*) using the LEaP module of the AMBER molecular modeling suite. LEaP places the ions sequentially in the electrostatic energy minimum, until the charge of the system is neutral; 22 ions are necessary for a duplex composed of 24 residues in total. Following ion placement, the ions were subjected to 100 steps of steepest descent minimization and 400 steps of conjugate gradient minimization with the duplex harmonically restrained to its initial coordinates by a force of 10 kcal/mol. Following ion minimization, the neutralized duplex was submitted to 1000 steps of steepest descent and 4000 steps of conjugate gradient minimization. At this point, the initial model structures were considered equilibrated with respect to ion placement, and production refinement commenced. Independently, the A and B models were subjected to 30 ps of simulated annealing. The SHAKE algorithm was applied to maintain idealized hydrogen bond and angle values (*40*). The parameter schedule applied during the simulated annealing process is included in the Supporting Information.

To increase conformational sampling, three runs per model structure were performed, with varying random number seeds. Following the simulated annealing, the final 5 ps of each of the six runs was averaged to form six average structures. Each of the six average structures was minimized for 200 steps of steepest descent and 800 steps of conjugate gradient minimization, with no restraints applied. Following minimization, all three minimized A structures were averaged together and all three B structures were averaged together, and the average structures were minimized without restraints for 100 steps of steepest descent and 400 steps of conjugate gradient minimization. Following minimization, the two structures were averaged together and minimized further, without restraints, for 500 steps of steepest descent and 2000 steps of conjugate gradient minimization. Following minimization, the average structure was refined with 20 ps of restrained molecular dynamics at room temperature. The parameter schedule used is included in Supporting Information. The final 5 ps of the room temperature rMD was averaged, minimized for 10 steps to repair averaging artifacts, and submitted to a final restrained minimization of 1000 steps of steepest descent and 4000 steps of conjugate gradient minimization. The final averaged, minimized structure was submitted to structure analysis using the DIALS and WINDOWS application which computes CURVES parameters (*41, 42*). Intermediate and final structures were analyzed for compliance with the experimental constraints using CORMA (*43*). The sixth root compliance values were 0.0702, 0.0585, and 0.0576 for the NOE cross-peak intensities from the 100, 150, and 200 ms NOESY experiments, reflecting excellent compliance of the final structure with the experimental data. Additional compliance data are included in Supporting Information.

Electrostatic Computations. The electrostatic contributions of the dC20 and dFdC20 residues were computed using Delphi (*44*). The calculation included only the partial charges from the dC20 and dFdC20 residues and no other charges from the molecules. Standard atomic radii were used for all charged atoms. The Delphi parameters used were 100 iterations of the QDIFFX routine. The dielectric constant of the helix interior was 1, and the dielectric constant of the helix exterior was 80. The surface was calculated using MSMS (*45*), and the electrostatic potential was mapped to the surface using trilinear interpolation. The result was visualized using the "DelphiViewer" extension of Chimera (UCSF).

RESULTS

NMR Analysis of Exchangeable ^1H. The exchangeable ^{1}H resonances of duplex DNA, RNA, or hybrid duplexes are informative concerning the formation and stability of specific base pairs in the duplex. Assignments for the imino and amino ^{1}H resonances of the G-C and A-T base pairs of [GEM] were obtained from analyses of 2D NOESY spectra in 95% H_2O solution (Supporting Information). The chemical shift assignments for the exchangeable ^{1}H resonances of [GEM] (Supporting Information) are similar to the corresponding position of [OKA], the model Okazaki fragment consisting of all native nucleotides (*23*). In particular, the imino resonance for G5, the base pairing partner of dFdC20 in [GEM], is shifted only slightly relative to the chemical shift of G5 base paired to dC in [OKA] (12.68 vs 12.55 ppm; *24*). Changes in chemical shift for other exchangeable ^{1}H resonances of [GEM], relative to [OKA], were of similar magnitude, suggesting that the duplexes had similar overall structure. The line widths for the T21 and T22 imino ^{1}H resonances of [GEM] were broadened, however, relative to the line widths observed for these resonances in [OKA] at identical temperatures, consistent with the DNA duplex region (DDR) of [GEM] being frayed and the imino ^{1}H resonances being exchange broadened. These results are consistent with thermodynamic measurements that reveal decreased global stability for [GEM] relative to [OKA] (Table 1).

Table 1: Thermodynamic Parameters for the Formation of [GEM] and [OKA] at 20 °C

oligomer	T_M (°C)[a]	ΔG^{CD}_{vH} (kcal/mol)	ΔH^{CD}_{vH} (kcal/mol)	$T\Delta S^{CD}_{vH}$ (kcal/mol)
[GEM]	41.2	−14	−94 (−76)[b]	−80
[OKA]	45.5	−14	−87 (−80)[b]	−73

[a] T_M extrapolated for a total strand concentration of 13.3 μM. [b] Comparison of van't Hoff enthalpies obtained from analysis of the shape of melting curves (in parentheses) and from T_M dependence on strand concentration.

Thermodynamic Measurements. The effects of dFdC substitution on the stability of the model Okazaki fragment [GEM] were investigated using temperature-dependent UV spectroscopy. The results are summarized in Table 1. The T_M for the dFdC-substituted duplex was 41.2 °C at a concentration of 13.3×10^{-6} M, a value 4.3 °C lower than for [OKA], the model Okazaki fragment consisting of only native nucleotides. The decreased stability caused by dFdC substitution was similar to that caused by cytarabine substitution (*23*). The free energies for formation of each duplex were the same, within experimental error (−14 kcal/mol). The relative enthalpic and entropic contributions to the free energy differed between the duplexes, however. The relative stabilizing contribution from the enthalpic term was greater for [GEM] than for [OKA], as measured from the concentration dependence of the T_M, but slightly greater for [OKA] than for [GEM] measured from the shape of the melting curve (van't Hoff enthalpy; Table 1). It is worth noticing that the enthalpic contributions for [OKA] obtained from the concentration dependence of T_M and from the shape of the melting curves are in good agreement, suggesting that this transition occurred in an all-or-none fashion. In the case of [GEM], the values obtained from these two approaches differ significantly from each other, which may indicate that the transition takes place through intermediate steps. The presence of a non-two-state transition makes it difficult to elucidate the source of the destabilization caused by dFdC substitution. However, the relative destabilizing contribution from the entropic term measured from the concentration dependence of the T_M was larger for [GEM] than for [OKA]. This indicates that the substitution of dFdC decreases duplex stability of the model Okazaki fragment, inducing better base pair stacking interactions and at the same time causing a local ordering of ions and water molecules at the substitution site. This is consistent with the observations in the solution structure of [GEM].

NMR of Nonexchangeable ^1H. The assignments for the nonexchangeable ^{1}H resonances of [GEM] were made using an approach similar to that described previously for the assignment of similar resonances for [OKA] (Supporting Information) (*24*). In particular, the ^{1}H resonance assignments for each of the 18 deoxyribose sugars were made using TOCSY and COSY experiments (Supporting Information). Stereochemical assignments for H2′/2″ were made on the basis of the relative intensities of the H1′−H2′/H2″ cross-peaks for NOESY spectra acquired with 100 ms mix time. H2″ resonated downfield of H2′ for all deoxyribose sugars except G5. Sequential connectivity between the deoxyribose spin systems was established by the observation of (*n*)H8/H6−(*n*)H1′ and (*n*)H8/H6−(*n*−1)H1′ and/or (*n*)H8/H6−(*n*)-H2′/H2″ and (*n*)H8/H6−(*n*−1)H2′/H2″ cross-peaks in the NOESY spectra. The ribose spin systems were assigned on the basis of (*n*)H1′−(*n*)H2′ and (*n*)H8/H6−(*n*−1)H2′ cross-peaks in NOESY spectra and H3′−H4′ cross-peaks in TOCSY and COSY spectra. Sequential connectivities for both types of nucleotides were also apparent from (*n*−1)-H8/H6−(*n*)H5/M cross-peaks in NOESY spectra. Assignment of adenosine H2 resonances were made on the basis of analysis of 2D NOESY data in both H_2O and D_2O solution. Each of the adenosine H2 resonances showed NOE cross-peaks either to the H1′ resonance of the 3′ neighbor (intrastrand) or to the H2 resonance of an adjacent adenosine, as well as to the imino ^{1}H of the base pairing partner dT.

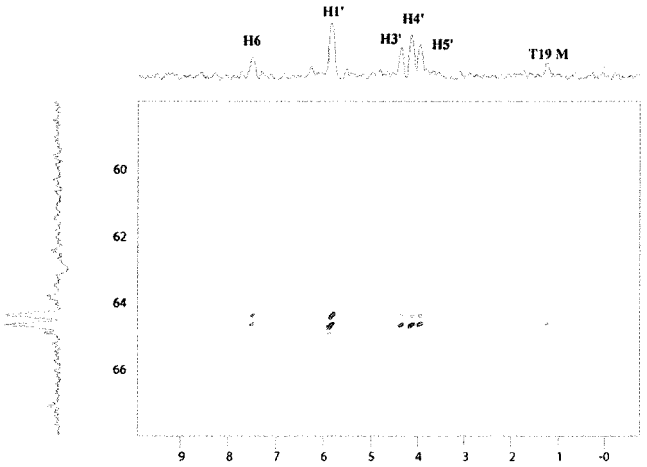

FIGURE 2: 2D ^{1}H−^{19}F HOESY of [GEM]. Cross-peaks are indicated for the intraresidue interaction of the geminal difluoro group of dFdC20 with H6, H1′, H3′, H4′, and H5′. Cross-peaks are also indicated for the interesidue interaction of F2′/F2″ with the methyl group of T19.

Structure of dFdC20. The NMR assignments for dFdC20 were established on the basis of NOESY cross-peaks between T21 H6 and dFdC20 H1′, dFdC20 H6 and T19 H1′, T19 H6 and dFdC20 H5, and T21 M to dFdC20 H6 (Supporting Information). The assignment of the geminal difluoro ^{19}F resonances of dFdC20 and additional interesidue assignments between dFdC20 and adjacent nucleotides were made from 2D HOESY spectra (Figure 2). The strongest HOESY cross-peaks were observed between the geminal difluoro resonances and dFdC20 H1′. Additional ^{1}H−^{19}F HOESY cross-peaks were also observed between dFdC20 H6, H3′, and H4′ and the geminal difluoro resonances of dFdC20 and between T19 M and the geminal difluoro group, suggesting efficient stacking of T19 and dFdC20. The HOE cross-peak between the geminal difluoro group and dFdC20 H4′ was slightly more intense than the corresponding cross-peak to dFdC20 H3′, a result consistent with a short interatomic F2″ to H4′ distance and with a small pseudorotation angle for the dFdC sugar ($P < 40°$). The HOESY information was used only qualitatively in making resonance assignments and was not used in determining distance or angular restraints that were used in the restrained molecular dynamics refinement procedure. Refinement of the structure using the ^{1}H NMR data in conjunction with restrained molecular dynamics using the AMBER force field resulted in dFdC20 adopting an A-form sugar pucker.

Substitution of dFdC for dC in duplex DNA, or a model Okazaki fragment, is expected to alter the biophysical properties of the nucleic acid in terms of both the structure

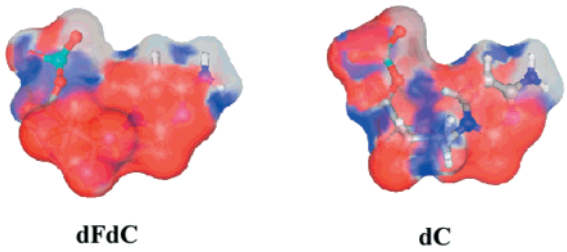

FIGURE 3: Electrostatic surface potential for dFdC and dC. Coordinates for each nucleotide were extracted from the NMR structures of [GEM] and [OKA] (*24*), respectively. Electrostatic potential was calculated using Delphi.

and the electrostatic potential in the vicinity of the site of substitution. The altered structural properties of the nucleic acid are expected to arise as a consequence of dFdC adopting an alternative conformation relative to the C2′-endo sugar pucker ordinarily adopted by dC in duplex DNA. The final refined structure for [GEM] is consistent with dFdC adopting an atypical C3′-endo conformation (Figure 1). In addition to altering the structure of [GEM], the geminal difluoro group of dFdC substantially alters the electrostatic surface at the site of substitution. The electrostatic surface of dFdC, calculated using Delphi, is shown in Figure 3. The corresponding surface of dC is also shown for comparison in Figure 3. Fluorine substitution slightly increases the dimensions of the van der Waals surface of dFdC, relative to dC; however, the electronegative fluorine atoms result in a substantially altered electrostatic potential over this surface (Figure 3). The altered electrostatic potential will, in turn, affect the composition of electrolytes in proximity to the site of substitution and potentially affect the affinity for dFdC-substituted DNA or both small molecules and cognate proteins.

Structure of [GEM]. The structure of [GEM] resulting from restrained molecular dynamics refinement based on the experimental NMR data is shown in Figure 4. Also shown in Figure 4 is the structure of [OKA], the model Okazaki fragment consisting of all native nucleosides (*24*). The overall RMSD between the structures is 2.18 Å; thus the overall similarity of the dFdC-substituted model Okazaki fragment is substantially more similar to [OKA] than was the case for the cytarabine-substituted model Okazaki fragment which had an overall RMSD of 4.1 Å (*24*). The structure of [GEM] was regionally similar to that previously reported for [OKA]. The structure consisted of three regions: a duplex DNA region (DDR; nucleotides 1−6 and 18−24), a hybrid duplex region (HDR; nucleotides 9−12 and 13−16), and a junction region (JR; nucleotides 7, 8, 17, and 18) (*24*). The most substantial differences in structure between [GEM] and [OKA] occurred at the site of substitution (dFdC20) and in the JR.

The structure of the DDR of [GEM] was highly similar to that of the DDR of [OKA] with a pairwise regional RMSD of 1.26 Å. The structure of the DDR of [GEM] is presented in the Supporting Information. The largest difference in this region between the two duplexes occurred at dFdC20, which had a sugar pucker of 20° compared to 130° for dC20 in [OKA]. The value of χ was also anomalously low for dFdC20 (205°) relative to dC20 in [OKA] (230°), but this is reasonable since χ and pucker are generally correlated. Plots of all torsion angles for the entire duplex are included

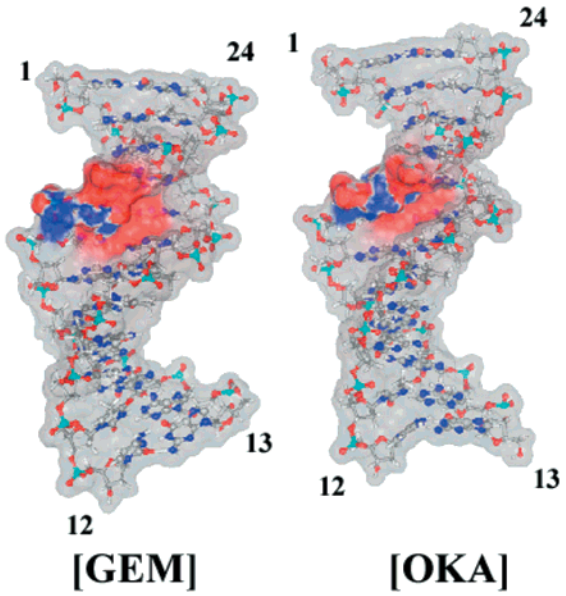

FIGURE 4: NMR structures of the dFdC-substituted model Okazaki fragment [GEM] and the native Okazaki fragment sequence [OKA] (*24*). All nucleotides except dFdC in [GEM] and dC in [OKA] are indicated as ball-and-stick figures. The electrostatic surface potential for dFdC and dC is indicated in each structure, respectively.

in the Supporting Information. These altered values for torsion angles in dFdC20, relative to dC20, were accommodated into the structure of the DDR with relatively minor changes to the conformations of other nucleotides. In particular, base stacking among adjacent purines in the DDR of [GEM] was not disrupted by the substitution of dFdC20. The DDR of [GEM] contains three consecutive A-T base pairs with the three adenosines consecutive in the DNA strand. These three adenosines (A2, A3, and A4) were efficiently base stacked in [OKA], as was apparent from NOE cross-peaks between H2 of A3 and H2 of both A4 and A2 (*24*). This efficient stacking of the purines was disrupted in the cytarabine-substituted model Okazaki fragment [ARAC], and the putative NOE cross-peak between A2 H2 and A3 H2 was not observed in the [ARAC] model Okazaki fragment (*24*). Efficient base stacking was apparent, based on observation of NOE cross-peaks for A3 H2 of [GEM] with both A2 H2 and A4 H2. Thus, the local conformation of dFdC20 did not disrupt helical stacking of contiguous purines in the DDR. In fact, dFdC20 substitution promoted helical stacking in the DDR as was evident by observation of an NOE cross-peak between A3 H8 and A2 H8 in [GEM] that was absent in [OKA]. Efficient base stacking among A2, A3, and A4 was observed in the NMR structure of [GEM], in accordance with the experimental observations (Supporting Information).

Although base stacking and overall geometry were similar for the DDR of [GEM] and [OKA], significant differences in stacking geometry between adjacent adenosines occurred in the junction region (JR) of [GEM] compared to the corresponding region of [OKA]. In particular, the NOE cross-peak observed between A18 H2 and A6 H2 in both [OKA] and [ARAC] was absent in [GEM], and the H2 resonances of A18 and A17 of [GEM] differed considerably in chemical shift from the corresponding values in both [ARAC] and [OKA]. The structural differences in the JR of [GEM] relative to [OKA] may contribute to the observed destabi-

lization of the duplex, with the decrease in melting point due to dFdC20 substitution being slightly greater than was observed for the cytarabine-substituted model Okazaki fragment [ARAC], relative to [OKA] (Table 1; *23*). Interestingly, although both dFdC and cytarabine substitution resulted in subtle changes in duplex structure near the site of substitution, they affected different regions of the duplex to a greater extent. Cytarabine, which actually adopted a more B-form sugar pucker in [ARAC] than was observed for dC in [OKA], affected base stacking in the DDR. dFdC, which adopted a more A-form sugar pucker in [GEM] than was observed for dC in [OKA], mainly affected geometry and base stacking in the JR of the model Okazaki fragment.

Electrostatics of [GEM]. The effects of nucleoside analogue substitution to the biophysical properties of the nucleic acid result from both conformational effects and changes in the electrostatic surface. As shown in Figure 3, dFdC presents a much more highly electronegative surface than dC as a consequence of the highly electronegative geminal difluoro group. The electrostatic surface of the entire model Okazaki fragment is altered near the site of dFdC substitution as shown in Figure 4. While the phosphate groups and electronegative atoms that line the minor groove of duplex nucleic acids create a highly electronegative surface for [OKA], the substitution of dFdC20 in [GEM] substantially increases the electronegativity of the surface. Thus, while the inherent malleability of nucleic acids might mute the relatively subtle structural differences arising from dFdC substitution in vivo, the substantial differences in electronegativity arising from dFdC substitution may be important in protein binding and other important nucleic acid-mediated processes.

DISCUSSION

In the present paper, we have described the effects of dFdC substitution to the structure, stability, and electrostatics of a model Okazaki fragment. These results enhance our understanding of the physicochemical basis for the alteration of DNA-mediated properties due to dFdC substitution that contribute to the anticancer activity of this drug. The present studies indicate that substantial differences occur between dFdC and dC with regard to the preferred nucleoside conformation, the relative charge distribution of the nucleoside, and the relative size of the nucleoside. Although the present studies do not permit delineation of which of these factors are most responsible for the poor DNA polymerase substrate properties of dFdCTP, or for the pausing of the polymerase following dFdC misincorporation, they demonstrate features of the DNA polymerase−dFdCTP complex, and of the nascent DNA following dFdCTP misincorporation, that likely contribute to reduced rates of dFdCTP misincorporation into DNA and for DNA polymerase pausing. For example, the NMR structure of [GEM] revealed that dFdC adopted a C3′-endo sugar pucker rather than the C2′-endo sugar pucker characteristic of dC in B-form DNA. Thus, presuming dFdCTP also preferred a C3′-endo sugar pucker, an energetic penalty would be associated with adoption of a C2′-endo sugar pucker by dFdCTP in the DNA polymerase−dFdCTP complex to permit appropriate stereochemical alignment of reactive groups to allow phosphodiester bond formation to proceed. Likewise, assuming dFdC also adopted a C3′-endo sugar pucker as the terminal nucleotide in the nascent DNA, an energetic penalty would be assessed for conformational rearrangement to a C2′-endo sugar pucker to permit proper alignment of reactive groups for phosphodiester bond formation for addition of the nucleotide following dFdCTP misincorporation.

In addition to altered conformational preferences affecting the rate of dFdCTP misincorporation and polymerase pausing, the electron-withdrawing geminal difluoro group significantly alters the electrostatic surface of the nucleoside. The altered electrostatic surface for dFdC, relative to dC, likely contributes to the reduced rate of misincorporation of dFdCTP into DNA and polymerase pausing. Altered electrostatics may affect complex formation between dFdCTP and DNA polymerase, possibly affecting the rate of dFdCTP misincorporation. Altered electrostatics may also effect adoption of the preferred orientation for the complex between nascent DNA and DNA polymerase. The electron-withdrawing effects of fluorine also decrease the electron density of the triphosphate and 3′-hydroxyl groups of dFdCTP, thus reducing the reactivity of these sites during phosphodiester bond formation and decreasing the reaction rate. In particular, the decreased electron density at the 3′-hydroxyl of dFdC in the nascent DNA chain is likely a substantial reason for the pausing of DNA polymerase following misincorporation of dFdCTP. In addition to conformational and electrostatic effects, fluorine substitution also alters the size of dFdCTP relative to dC, and steric clashes may also contribute to the pausing of DNA polymerase following dFdCTP misincorporation.

The cytotoxicity of dFdC is highly correlated with misincorporation of dFdCTP into DNA. Although dFdC misincorporation affects DNA polymerase processivity, dFdC is found predominantly in internucleotide linkages in DNA (*15*). Thus the anticancer activity of dFdC appears to arise mainly as a consequence of alterations in DNA-mediated processes following dFdCTP misincorporation and not as a result of alterations in DNA polymerase activity. The present study demonstrates that dFdC substitution alters the local structure of the DNA duplex region of a model Okazaki fragment. These results are consistent with conformational changes in DNA resulting from dFdCTP misincorporation as being responsible, in part, for the DNA-mediated effects of dFdC. In this regard, the dC analogue cytarabine, a potent antileukemic agent, interferes with top1-mediated cleavage of DNA (*18*). The same properties described above as contributing to reduced misincorporation of dFdCTP into DNA and DNA polymerase pausing also likely contribute to alterations in DNA-mediated processes due to dFdCTP misincorporation. At present, it is not possible to delineate the separate effects of altered structure, decreased stability, altered electrostatics, and changes in size to alterations in DNA-mediated processes. Nonetheless, the present results are consistent with alterations to the biophysical properties of dFdC-substituted DNA contributing to the anticancer activity of this drug.

ACKNOWLEDGMENT

The authors thank Junmei Wang (UCSF) for assistance in preparing the point charges and determining the fluorine bond parameters for dFdC. W.H.G. is grateful to the CCCWFU for a PUSH grant.

SUPPORTING INFORMATION AVAILABLE

Tables of chemical shifts for the exchangeable and nonexchangeable ^{1}H of [GEM], 2D NMR spectra used in making the assignments of [GEM], figures of the DDR and JR of [GEM], a summary of the torsion angles and helical parameters for the model Okazaki fragment, and a restraint file used in refinement and summary compliance with experimental data. This material is available free of charge via the Internet at http://pubs.acs.org.

REFERENCES

1. Seidman, A. D. (2001*) Oncology 60*, 189−198.
2. Greggi, S., Salerno, M. G., D'Agostino, G., Ferrandina, G., Lorusso, D., Manzione, L., Mancuso, S., and Scambia, G. (2000) *Oncology 60*, 19−23.
3. Illiano, A., Barletta, E., de Marino, V., Battiloro, C., Barzelloni, M., Scognamiglio, F., Rossi, N., Zampa, G., de Bellis, M., and Gridelli, C. (2000) *Anticancer Res. 20*, 3999−4004.
4. Burris, H. A., III, Moore, M. J., Andersen, J., Green, M. R., Rothenberg, M. L., Modiano, M. R., Cripps, M. C., Portenoy, R. K., Storniolo, A. M., Tarassoff, P., Nelson, R., Dorr, F. A., Stephens, C. D., and Von Hoff, D. D. (1997) *J. Clin. Oncol. 15*, 2403−2413.
5. Fracasso, P. M., Tan, B. R., Jr., Grieff, M., Stephenson, J. S., Jr., Liapis, H., Umbeck, N. L., Von Hoff, D. D., and Rowinsky, E. K. (1999) *J. Natl. Cancer Inst. 91*, 1779−1780.
6. Seidman, A. D. (2001) *Oncology 15*, S11−S14.
7. Heinemann, V. (2001) *Oncology 60*, 8−18.
8. Peters, G. J., van der Wilt, C. L., van Moorsel, C. J. A., Kroep, J. R., Bergmann, A. M., and Ackland, S. P. (2000) *Pharmacol. Ther. 87*, 227−253.
9. Bunn, P. A., Jr., and Kelly, K. (1998) *Clin. Cancer Res. 5*, 1087−1100.
10. Von der Maase, H. (2000) *Eur. J. Cancer 36*, S13−S16.
11. Van Moorsel, C. J. A., Pinedo, H. M., Veerman, G., Bergman, A. M., Kuiper, C. M., Vermorken, J. B., Van der Vijgh, W. J. F., and Peters, G. J. (1999) *Br. J. Cancer 35*, 808−814.
12. Plunkett, W., Huang, P., Xu, Y. X., Heinemann, V., Grunewald, R., and Gandhi, V. (1995) *Semin. Oncol. 22* (Suppl. 11), 3−11.
13. Heinemann, V., Schulz, L., Issels, R. D., and Plunkett, W. (1995) *Semin. Oncol. 22* (Suppl. 11), 11−18.
14. Plunkett, W., Huang, P., Searcy, C. E., and Gandhi, V. (1996) *Semin. Oncol. 23*, 3−15.
15. Huang, P., Chubb, S., Hertel, L. W., Grindley, G. B., and Plunkett, W. (1991) *Cancer Res. 51*, 6110−6117.
16. Lawrence, T. S., Davis, M. A., Hough, A., and Rehemtulla, A. (2001) *Clin. Cancer Res. 7*, 314−319.
17. Heinemann, V., Schulz, L., Issels, R. D., and Plunkett, W. (1997) *Semin. Oncol. 22*, 11−18.
18. Pourquier, P., Takebayashi, Y., Urasaki, Y., Gioffre, C., Kohlhagen, G., and Pommier, Y. (2000) *Proc. Natl. Acad. Sci. U.S.A. 97*, 1885−1890.
19. Kufe, D. W., Munroe, D., Herrick, D., Egan, E., and Spriggs, D. (1984) *Mol. Pharmacol. 26*, 128−134.
20. Ross, D. D., Cuddy, D. P., Cohen, N., and Hensley, D. R. (1992) *Cancer Chemother. Pharmacol. 31*, 61−70.
21. Meyers, M., Wagner, M. W., Hwang, H.-S., Kinsella, T. J., and Boothman, D. A. (2001) *Cancer Res. 61*, 5193−5201.
22. Gmeiner, W. H. (1998) *Curr. Med. Chem. 5*, 115−135.
23. Gmeiner, W. H., Skradis, A., Pon, R. T., and Liu, J.-Q. (1998) *Nucleic Acids Res. 26*, 2359−2365.
24. Gmeiner, W. H., Konerding, D., and James, T. L. (1999) *Biochemistry 38*, 1166−1175.
25. Sahasrabudhe, P. V., Pon, R. T., and Gmeiner, W. H. (1995) *Nucleic Acids Res. 23*, 3916−3921.
26. Sahasrabudhe, P. V., Pon, R. T., and Gmeiner, W. H. (1996) *Biochemistry 35*, 13597−13608.
27. Richardson, F. C., Richardson, K. K., Kroin, J. S., and Hertel, L. W. (1992) *Nucleic Acids Res. 20*, 1763−1768.
28. Marky, L. A., and Breslauer, K. J. (1987) *Biopolymers 26*, 1601−1620.
29. Cantor, C. R., Warshaw, M. M., and Shapiro, H. (1970) *Biopolymers 9*, 1059−1077.
30. Marky, L. A., Blumenfeld, K. S., Kozlowski, S., and Breslauer, K. J. (1983) *Biopolymers 22*, 1247−1257.
31. Hore, P. J. (1983) *J. Magn. Reson. 55*, 283−300.
32. States, D. J., Haberkorn, R. A., and Ruben, D. J. (1982) *J. Magn. Reson. 48*, 286−292.
33. Griesinger, C., Sorenson, O. W., and Ernst, R. R. (1985) *J. Am. Chem. Soc. 107*, 6394−6396.
34. Stott, K., and Keeler, J. (1996) *Magn. Reson. Chem. 34*, 554−558.
35. Borgias, B. A., and James, T. L. (1990) *J. Magn. Reson. 87*, 475−487.
36. Huang, C. C., Couch, G. S., Pettersen, E. F., and Ferrin, T. E. (1996) *Pacific Symp. Biocompu*t. *1*, 724.
37. Case, D. A., Pearlman, J. W., Caldwell, T. E., Cheatham, W. S., III, Ross, C. L., Simmerling, T. A., Darden, K. M., Merz, R. V., Stanton, A. L., Cheng, J. J., Vincent, M., Crowley, D. M., Ferguson, R. J., Radmer, G. L., Seibel, U. C., Singh, P. K., Weiner, S. J., and Kollman, P. A. (2000) *AMBER 6*, University of California, San Francisco.
38. Wang, J., Wang, W., and Kollman, P. A. (2001) *J. Comput. Chem*. (in press).
39. Singh, U. C., Weiner, S. J., and Kollman, P. A. (1985) *Proc. Natl. Acad. Sci. U.S.A. 82*, 755−759.
40. Ryckaert, J. P., Cicotti, G., and Berendsen, H. J. C. (1977) *J. Comput. Phys. 23*, 327−341.
41. Ravishanker, G., Swaminathan, S., Beveridge, D. L., Lavery R., and Sklenar, H. (1989) *J. Biomol. Struct. Dyn. 6*, 669−699.
42. Lavery, R., and Sklenar, H. (1989) *J. Biomol. Struct. Dyn. 6*, 655−667.
43. Borgias, B. A., and James, T. L. (1988) *J. Magn. Reson. 79*, 492−512.
44. Nicholls, A., and Honig, B. (1991) *J. Comput. Chem. 12*, 435−445.
45. Sanner, M. F., Olson, A. J., and Spehner, J.-C. (1995) *Proc. 11th ACM Symp. Comput. Geom*., C6−C7.

BI015678L